Numerical Modeling for Tunnel Lining Optimization

Jose Francisco Suarez Fino * and Juan Manuel Mayoral Villa *

Posted Date: 16 July 2024

doi: 10.20944/preprints202407.1329.v1

Keywords: Tunnel; numerical modeling; primary lining; optimization primary lining; load-transfer mechanism; conventional excavation; back-analyses; FLAC^{3D}

Article

Numerical Modeling for Tunnel Lining Optimization

JF Suárez/Fino * and JM Mayoral/Villa *

[1] Geotechnical Department, Institute of Engineering, National University of Mexico, Mexico City, Mexico
* Correspondence: (email:jfsuarezfino@consultecingenieria.mx, and francisco_suarez_fino@yahoo.com); email: jmayoralv@iingen.unam.mx)

Abstract: The construction of tunnels excavated by the conventional method in densely populated urban environments requires an adequate characterization of the loads acting on the primary lining during the excavation process to ensure that the ground is deformed and stresses around the tunnel are relieved, simultaneously complying with the failure and serviceability limits of international standards while minimizing damage to nearby structures. In this paper, common lining design criteria are revisited, through the numerical simulation of an instrumented tunnel section which is part of a 4.5 km long metro line currently under construction in Mexico City. Key needs for improvement in current design approaches are identified. The tunnel was instrumented with load cells, extensometers, and topographical references for convergences and divergences. A three-dimensional finite difference model of the instrumented section was developed, and the load transfer mechanisms between the excavated soil and the primary lining was analyzed. Then, the numerical simulation of the contribution of the secondary lining in the overall stability for sustained load was established, along with the expected ground settlements, which can significantly affect nearby structures. Results gathered from this research are key for updating lining design criteria for urban tunnels built in stiff brittle soils.

Keywords: Tunnel; numerical modeling; primary lining; optimization primary lining; load-transfer mechanism; conventional excavation; back-analyses; FLAC^{3D}

1. Introduction

As stablished by Mayoral et al., (i.e., Mayoral et al., 2014 & 2015), modern tunnel design in densely populated areas, such as Mexico City, requires to revise both state limit of failure (i.e., factors of safety for tunnel face and general stability), and service (i.e., ground deformations in the proximity of the tunnel at surface and within the tunnel) simultaneously, to avoid potential catastrophic collapse (e.g., de Ágreda, 2019; Oliver, 1994, 1995; Sousa & Einstein, 2021), or damage in nearby structures related to differential settlements (e.g., Mayoral et al., 2015; Son, 2015, 2016; Dong et al., 2022; Lim et al., 2023). This is particularly important when excavating with the conventional tunnelling method, CT, (ITA, 2009), in heavily populated urban areas.

A key design issue that strongly controls both state limits is the soil-tunnel lining interaction, which is mostly a function of the tunnel cross section geometry, lining thickness, structural configuration (i.e., one or two linings comprised for instance of shotcrete, reinforced concrete, steel frames), and recommended advancement length.

Several analytically-derived approaches are available in the technical literature to study soil-tunnel lining interaction, ranging from conventional methodologies, based on pressure of loose ground (e.g., Bierbaumer, 1913; Szechy, 1970; Terzaghi, 1946), relative stiffness solution (e.g., Einstein & Schwartz, 1979), characteristics ground curves (e.g., Ghorbani & Hasanzadehshooiili, 2019; Oreste, 2009; Panet et al., 2001), support reaction curves (e.g., Oreste, 2003; Verman et al., 1995; Wang & Luo, 2020), and longitudinal displacement curves, LDP, (e.g., Sadeghiyan et al., 2016; Vlachopoulos & Diederichs, 2009). Recently, more sophisticated approaches using numerical modelling of the coupled soil-tunnel lining interaction are also employed (e.g., Mayoral et al., 2014; Pitilakis et al., 2014; Argyroudis 2017; Mayoral et al., 2020; Mayoral and Mosqueda, 2021).

 doi:10.20944/preprints202407.1329.v1

Although several researchers have attempted to study the soil-tunnel lining interaction through instrumentation of actual tunnels (e.g., Karakus and Fowell, 2005; Zhang et al., 2013; He et al., 2019), and centrifuge tests models (e.g., Nomoto et al., 1999; Ng et al. 2013; Song and Marshall 2020), to date, there is still a lack of information regarding the soil-lining interaction during conventional tunneling in stiff cemented soils, which in turn, it is needed to assess the validity, and areas of improvement of current design methodologies.

This paper presents an in-depth study, using numerical modeling and instrumentation, of the soil-tunnel lining interaction in a tunnel during conventional excavation, aiming at assessing the lining performance, while seeking for potential optimization of the lining thickness. The tunnel is part of a metro extension currently under construction in Mexico City. The results gathered were compared with those estimated using some of the most used analytical conventional design methods, to identify its main limitations. Finally, once the proposed approach was validated, the efficiency of different lining alternatives was revised according to the global tunnel performance, considering both composite lining (i.e., primary and secondary lining) and single lining, establishing an optimal tunnel lining design for the case studied.

2. Case Study

The studied case was presented by Mayoral et al., (2023), and consist of a10m-diameter shallow urban tunnel, 4.5 km long, currently under construction in the western portion of Mexico City. **Error! Reference source not found.** shows the tunnel trace and instrumented tunnel segment. The tunnel runs within the so-called Tarango formation, which is mostly composed of highly cemented silty sands and dense to very dense sandy silts with varying degree of cementation. Thus, shear strength and compressibility parameters varied widely.

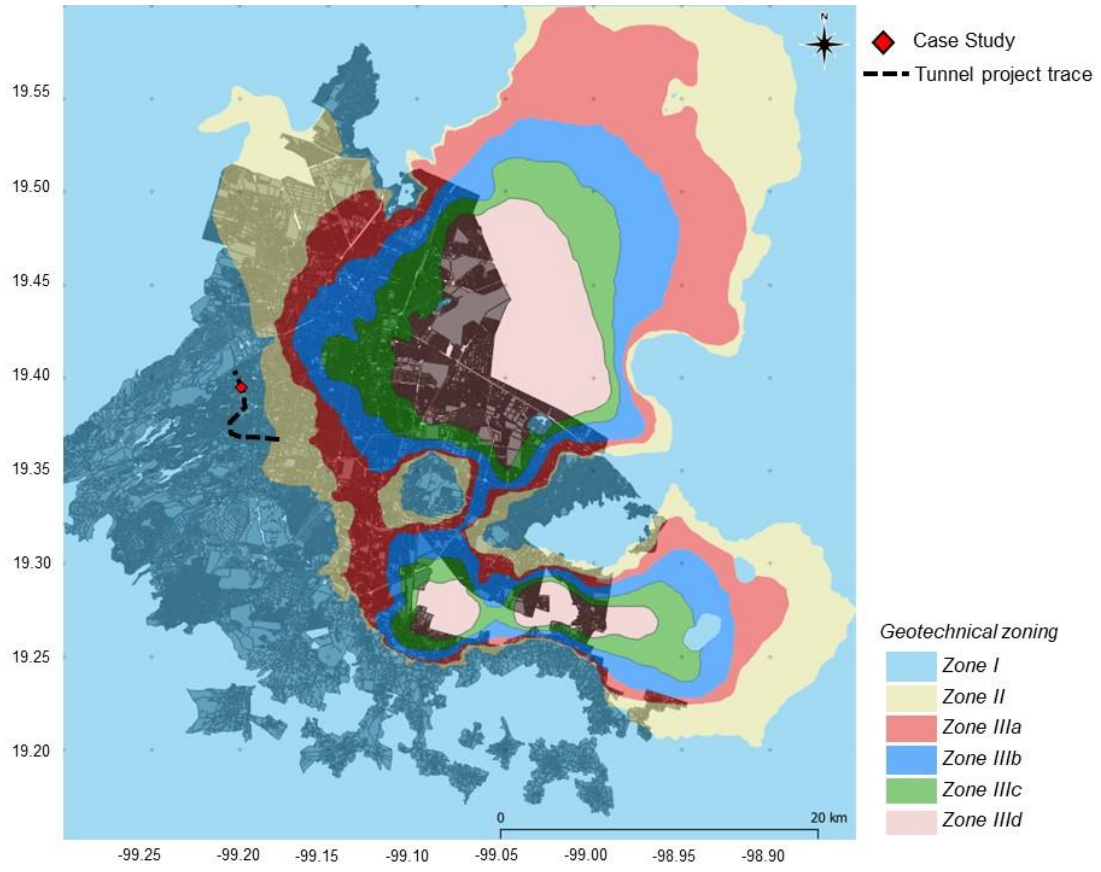

Figure 1. Project trace and geotechnical zoning of Mexico City.

 doi:10.20944/preprints202407.1329.v1

2.1. Geotechnical Conditions

Four standard penetration tests SP-1, SP-2, SP-3, and SP-4 were conducted at the site to characterize the subsurface conditions. The average exploration depth was around 40m. In addition, index properties were obtained from disturbed samples retrieved at several depths, which were used to establish the geotechnical units according to the Unified Soil Classification System, USCS. Strength and deformability parameters were determined from unconfined compression tests and triaxial UU tests conducted in undisturbed samples, as well as in-situ phicometer and pressuremeter tests. **Error! Reference source not found.** shows the soil profile characterization. In addition, empirical correlations (Hettiarachchi & Brown, 2009) based on SPT blow counts (N_{SPT} values) were also used to determine strength and deformability parameters (i.e., cohesion c, internal friction angle φ, and Young's Modulus at 50% strain E_{50}). In the cases where N_{SPT} values were larger than 50, the values used in the correlation were extrapolated according to the LRFD Bridge Design Specifications (2012) AASHTO (Eq. 1).

$$N_{SPT} = \frac{(50+N_2)*30}{15+N_3} \quad (1)$$

Where:

N_2 and N_3 are second and third advances of the standard penetration test

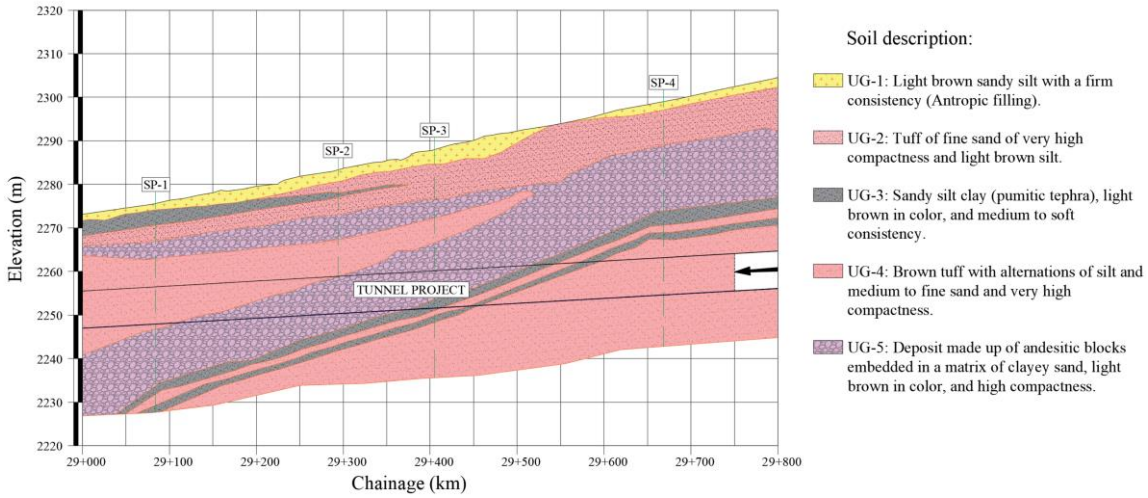

Figure 2. Soil profile and tunnel at the studied site.

The geotechnical properties of the soil profile estimated initially are summarized in **Error! Reference source not found.**Table 1. Poisson's ratio ν was defined from typical values for similar materials. The water table was not detected until the maximum explored depth.

Table 1. Initial geotechnical properties at the studied site estimated with correlations.

Layer	USCS	N_{SPT} (blows counts)	γ (kN/m³)	c (kPa)	φ (°)	E_{50} (MPa)	ν (-)
UG-1	ML	42	15.8	18	28	120.8	0.32
UG-2	SM	167	18.2	45	29	900.4	0.28
UG-3	CL-ML	40	17	13	27	97.5	0.34
UG-4	ML	126	18.2	40	28	470.5	0.28

 doi:10.20944/preprints202407.1329.v1

UG-5	SC	80	19.2	33	31	303.2	0.27

Where: N_{SPT}= extrapolated number of standard penetration tests blows counts; γ= unit weight; c= cohesion, φ= friction angle; E_{50}= Young's modulus at 50% strain; ν= Poisson ratio.

2.2. Tunnel Geometry and Excavation Process

The tunnel geometry is shown in **Error! Reference source not found.**. It was projected to have an external width of 10.6 m and external height of 8.50 m. The construction sequence considers three partial excavations: 1) upper-middle section, 2) central bench, and 3) lateral benches alternately. The primary lining, PL, is comprised of a 20 cm thick layer of steel fiber reinforced shotcrete, SFRS, f'c=25 MPa. The secondary lining, SL, consisted of a 40 cm thick reinforced concrete support with design strength after 28 days of f'c, 30 MPa.

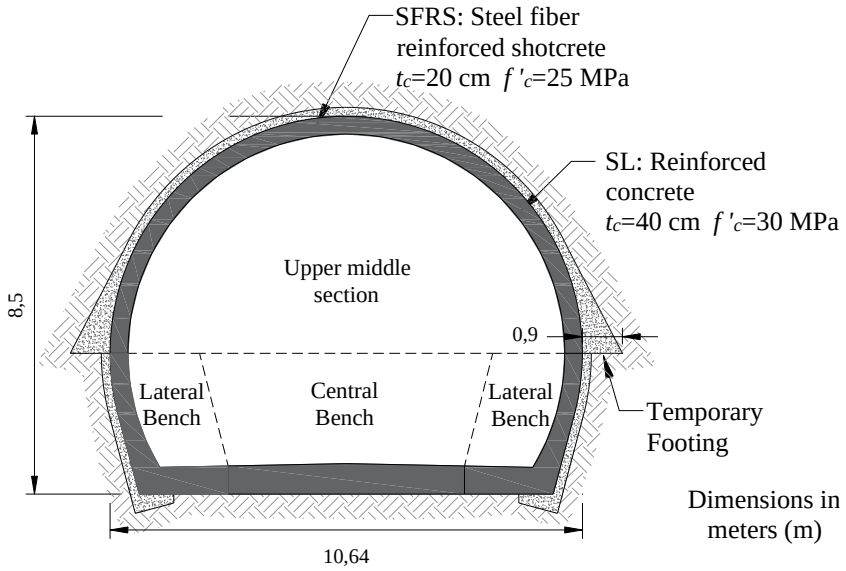

Figure 3. Tunnel cross-section and primary lining configuration used.

An schematic representation of the tunnel excavation process is depicted in **Error! Reference source not found.**, it consists of four main stages: 1) excavation of the upper-middle section with lengths of excavation phase of 1.0 m stabilizing the ground through the primary lining, leaving a central pillar unexcavated to reduce the risk of tunnel face failure, 2) once an excavation length of the upper-middle section of 35 m has been reached, the excavation of the central bench begins (stage 2), first a 9 m long work ramp is built and behind it, the central bench is completed, 3) when a distance of 35 m of excavation of the central bench is reached, measured from the beginning of the ramp, the alternate excavation of the lateral banks with advances of 3.0 m is started, stabilizing them employing a 20 cm thick layer of shotcrete reinforced with steel fibers, and 4) reinforcement and casting of the footings and sidewalls of the secondary tunnel lining, having an advance of 20 m, the secondary lining of reinforced concrete is implemented in the vault. Simultaneously, the reinforcement and casting of the bottom slab is carried out to close the tunnel ring. **Error! Reference source not found.** shows the excavation of the upper half of the section complete with the central core, highlighting the adverse ground conditions; poor soil quality and the presence of water seepage are observed.

Preprints.org (www.preprints.org) | NOT PEER-REVIEWED | Posted: 16 July 2024 doi:10.20944/preprints202407.1329.v1

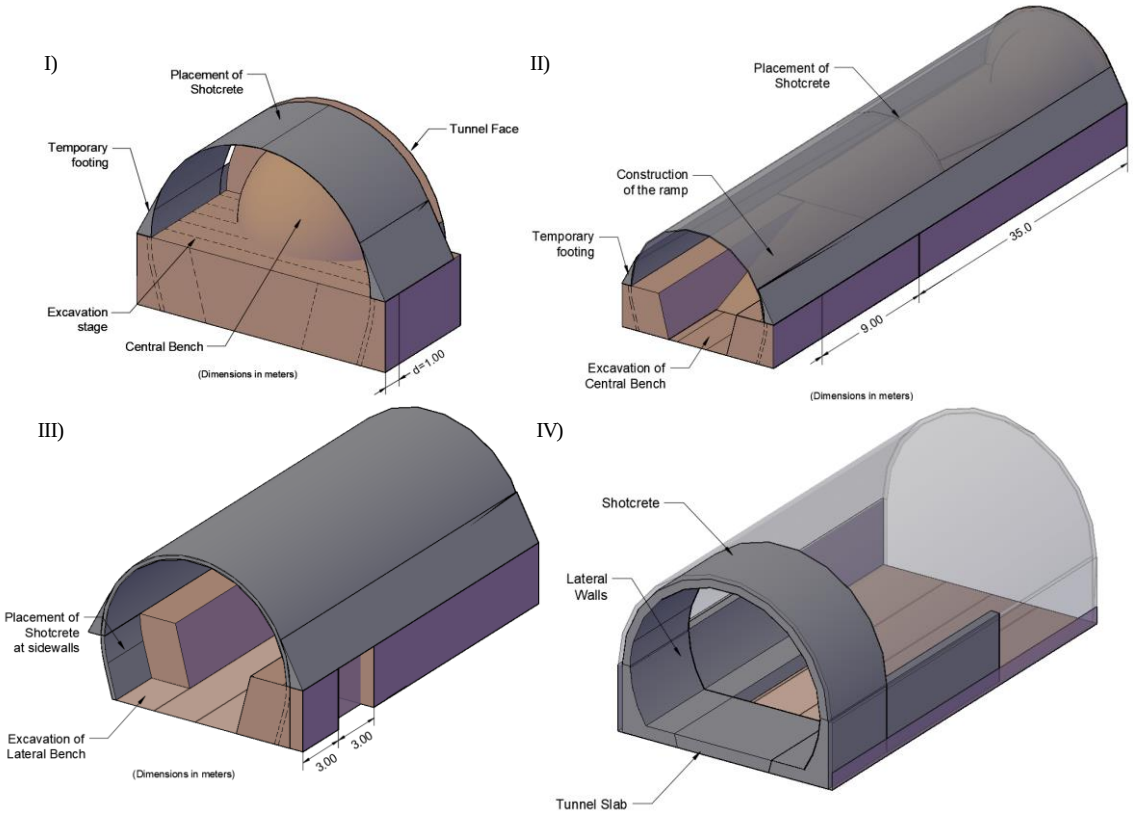

Figure 4. Schematic tunneling process (Mayoral et al., 2020).

Figure 5. Excavation of the complete upper half section with central core. It shows the poor quality of the soil and the presence of water seepage.

3. Tunnel Instrumentation

As depicted in **Error! Reference source not found.**a, five control points were placed within the tunnel to measure tunnel cross-section distortion (i.e., convergences and divergences). The control points were installed every 30 m, immediately after the construction of the primary lining, PL. These measurements were complemented with reference surface points to monitor the settlements along the tunnel axis. In addition, a tunnel section (29+300) was instrumented with one extensometer, radial, and tangential pressure cells to establish the load acting on the PL. First, an extensometer was installed before the excavation face reached the instrumented section. Then, radial pressure cells, RPC, were installed between the ground and the shotcrete of the primary lining, SFRC, to measure the radial stress, and tangential pressure cells, TPC, were embedded within the shotcrete to measure the axial stresses. **Error! Reference source not found.**b shows the configuration of the reference

 doi:10.20944/preprints202407.1329.v1

surface points installed to monitor the settlements along the tunnel axis. Topographical survey of both the primary and secondary lining was carried out to establish convergences and divergences. **Error! Reference source not found.** presents a summary of the installed sensors.

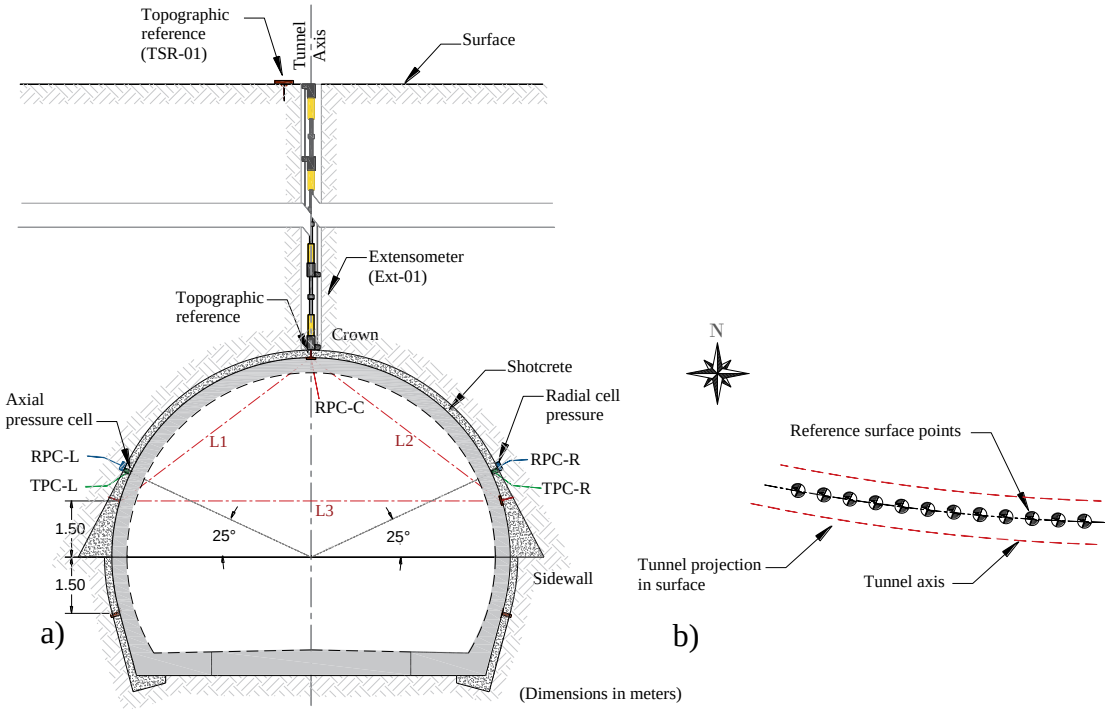

Figure 6. Schematic representation of the tunnel instrumentation: (a) inside the tunnel and (b) topographical elevation survey references, modified from (Mayoral et al., 2020).

Table 2. Instrumentation sensors and variable measured.

Sensor ID	Instrumentation	Variable measured
L1, L2 and L3	Convergences and divergences	Tunnel distortion
TSR-01	Reference surface points	Surface settlements
Ext-01	Extensometer	Tunnel crown settlements
RPC-L, RPC-R and RPC-C	Radial pressure cells	Radial stress on primary lining
TPC-L and TPC-R	Tangential pressure cells	Axial stress on primary lining

The following figures show photographs of the installation and measurement of the instruments.

 doi:10.20944/preprints202407.1329.v1

Figure 7. Drilling for the installation of the extensometer and measurement of the instrument.

Figure 8. Measurement of convergences during the excavation of the upper half section.

Figure 9. Maneuvers during the instrumentation of radial cells.

 doi:10.20944/preprints202407.1329.v1

Figure 10. Finally, the pressure transducers are protected with steel ducts for their protection and are channeled to the Datalogger where they are connected.

Figure 11. Placement of the first layer of shotcrete with 10 cm thick fibers, covering the periphery of the tunnel vault and the instrumented radial pressure cells.

Finally, **Error! Reference source not found.** shows the installation of the instruments to the Datalogger and the first reading of each of the instruments installed in the primary lining.

 doi:10.20944/preprints202407.1329.v1

Figure 12. Photograph showing the connection of the instruments to the Datalogger. Once connected, the first readings are taken on a Laptop using the Logger Net software.

Error! Reference source not found. presents measured vertical ground movements at tunnel crown at the control section, considering the settlement measured by the extensometer. It can be observed that when the excavation front is 7 tunnel diameters away (70 m), the impact on the deformation of the instrumented tunnel cross section is negligible. **Error! Reference source not found.**, **Error! Reference source not found.**, **Error! Reference source not found.**, **Error! Reference source not found.**, **Error! Reference source not found.**, **Error! Reference source not found.** y **Error! Reference source not found.** present the values measured at the convergence stations placed before and after the control section. Similarly, the excavation effect on surface ground settlement at the control section is quite low when the distance to the excavation faces reaches 7 tunnel diameters (**Error! Reference source not found.**). Figure 1 depicts the extensometer measurements. In this case, the effect of the excavation is less significant after the excavation face is at 3.5 diameters away from the instrumented site. **Error! Reference source not found.** shows the history of radial pressures recorded at the tunnel crown and walls. On the other hand, **Error! Reference source not found.** shows the history of tangential pressures recorded at the tunnel wall.

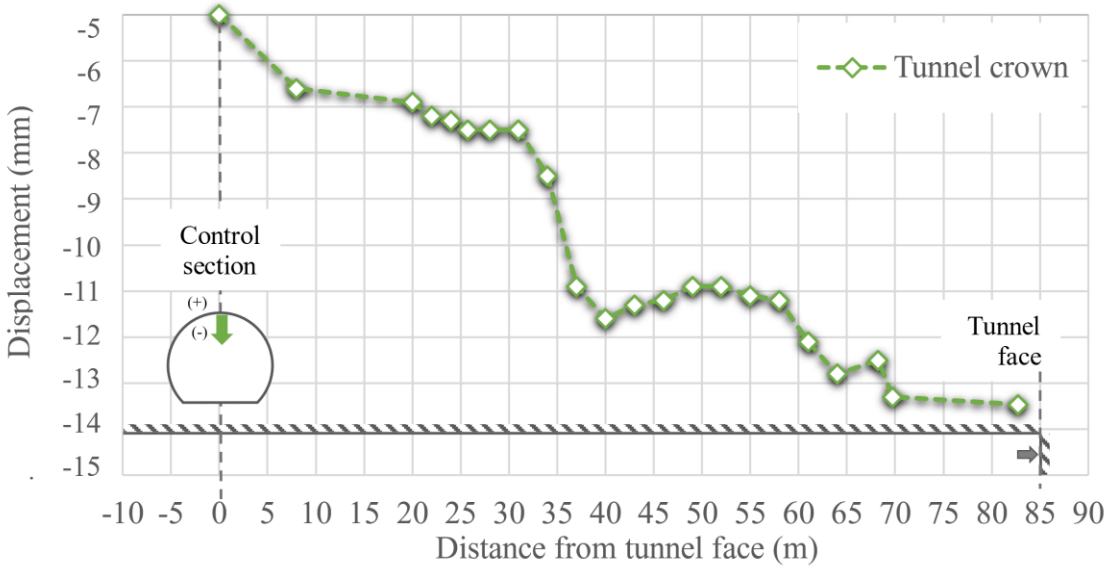

Figure 13. Measured vertical ground movements at tunnel crown in the control section.

Preprints.org (www.preprints.org) | NOT PEER-REVIEWED | Posted: 16 July 2024 doi:10.20944/preprints202407.1329.v1

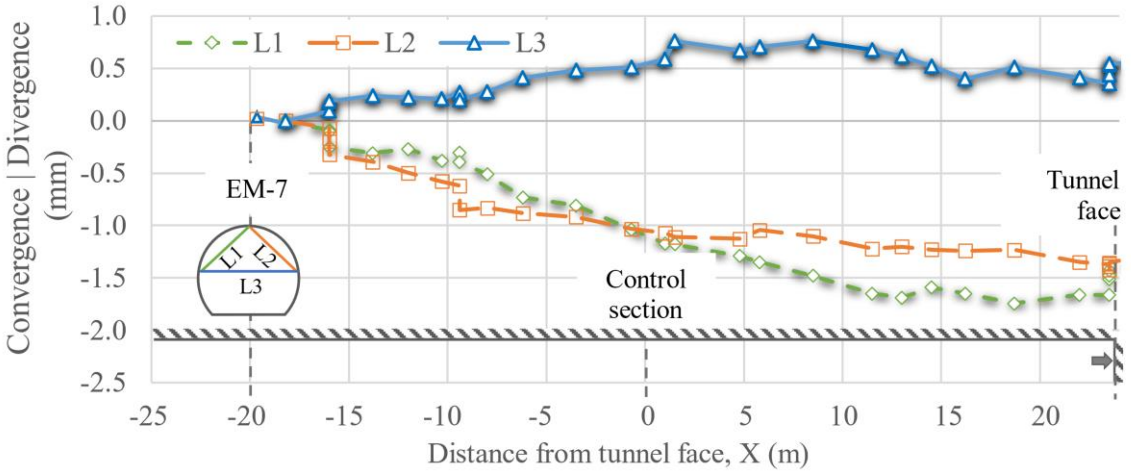

Figure 14. Convergences and divergences, EM-7, located 20 m before the control section.

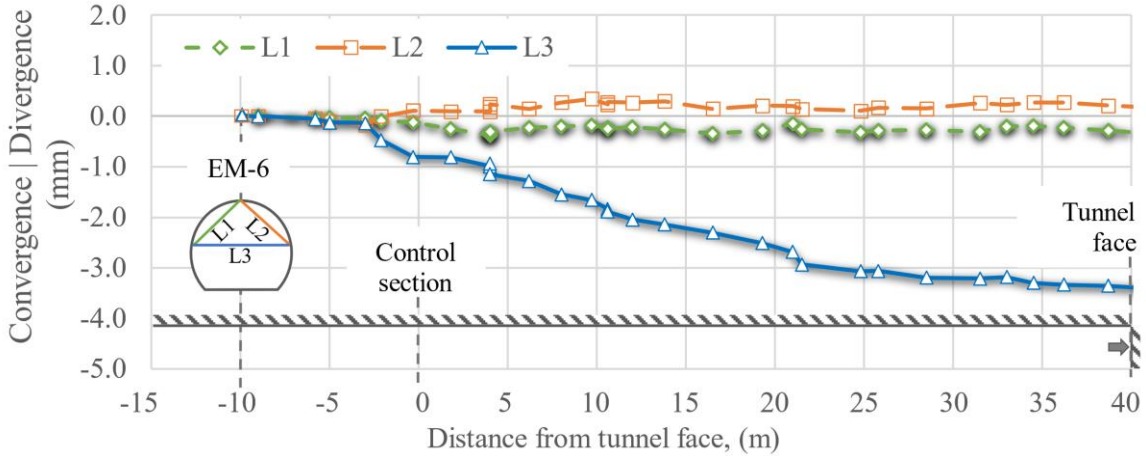

Figure 15. Convergences and divergences, EM-6, located 10 m before the control section.

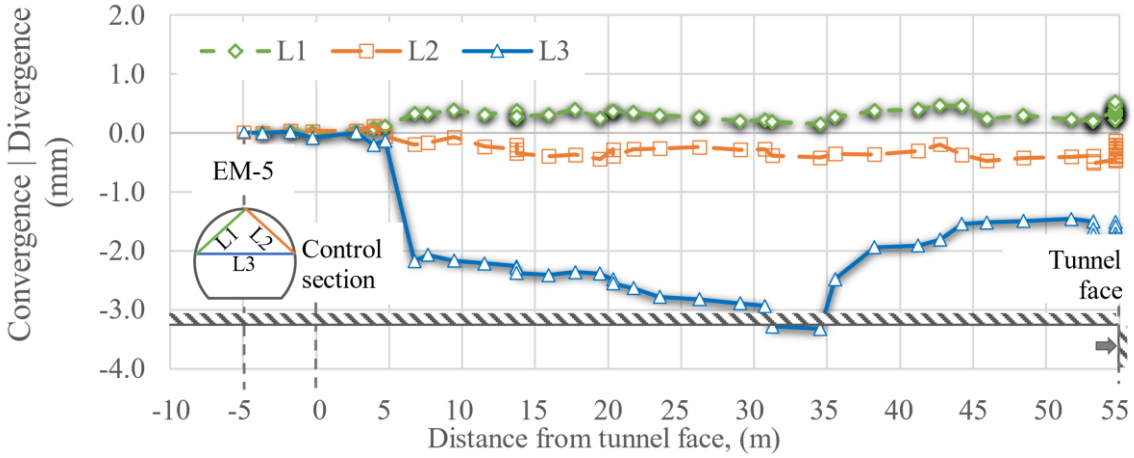

Figure 16. Convergences and divergences, EM-5, located 5 m before the control section.

Preprints.org (www.preprints.org) | NOT PEER-REVIEWED | Posted: 16 July 2024 doi:10.20944/preprints202407.1329.v1

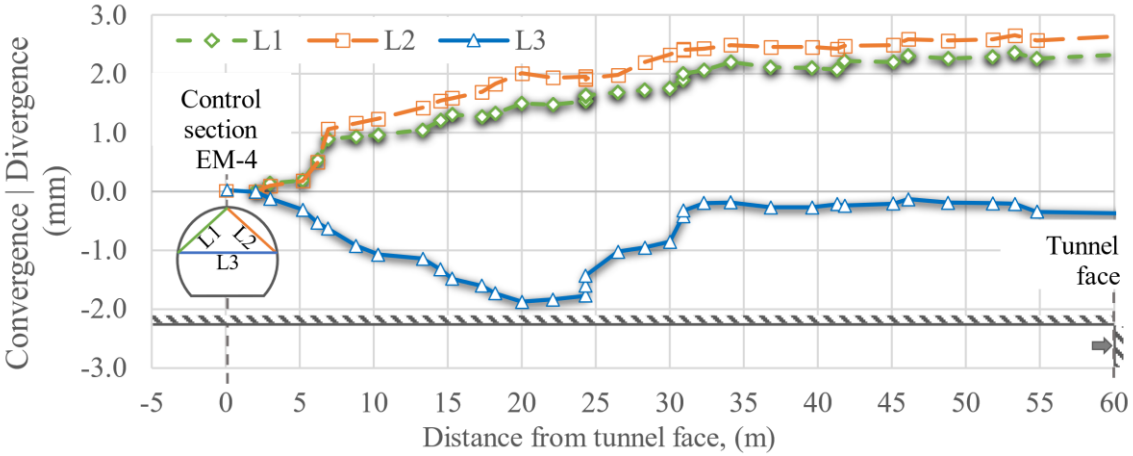

Figure 17. Convergences and divergences, EM-4, located at the control section.

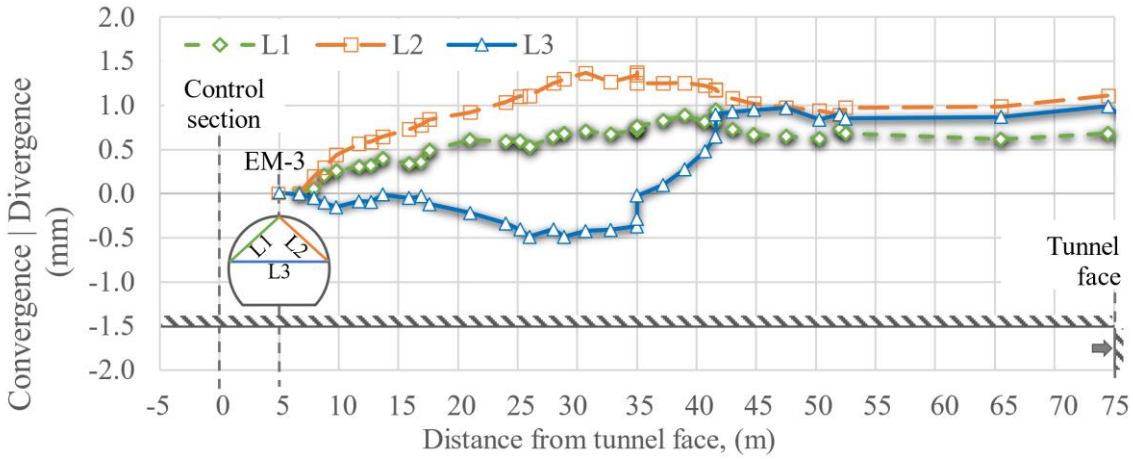

Figure 18. Convergences and divergences, EM-3, placed 5 m after the control section.

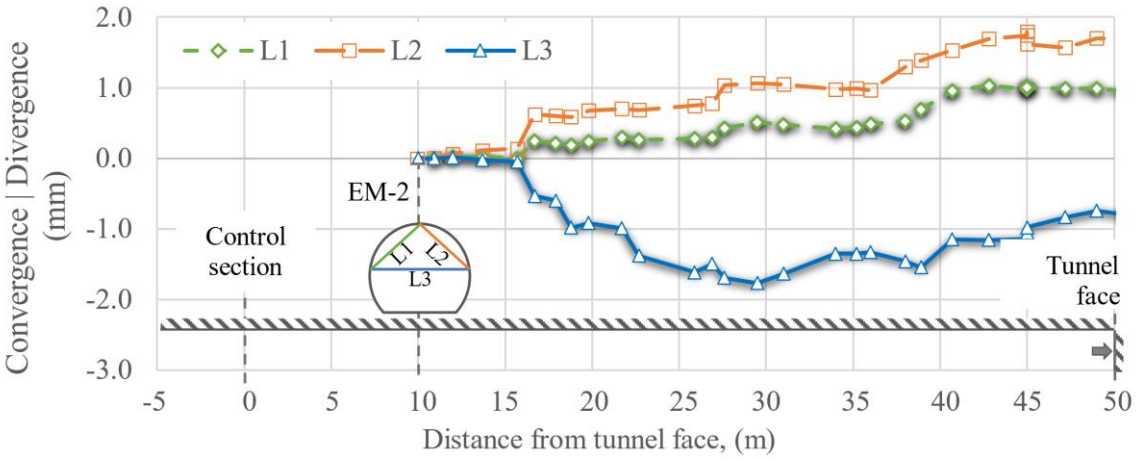

Figure 19. Convergences and divergences, EM-2, placed 10 m after the control section.

Preprints.org (www.preprints.org) | NOT PEER-REVIEWED | Posted: 16 July 2024 doi:10.20944/preprints202407.1329.v1

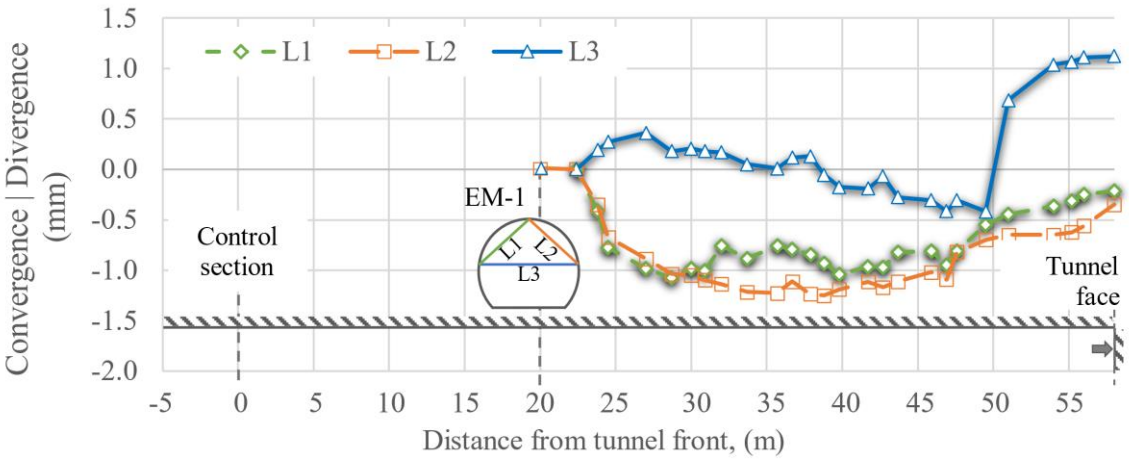

Figure 20. Convergences and divergences, EM-1, placed 20 m after the control section.

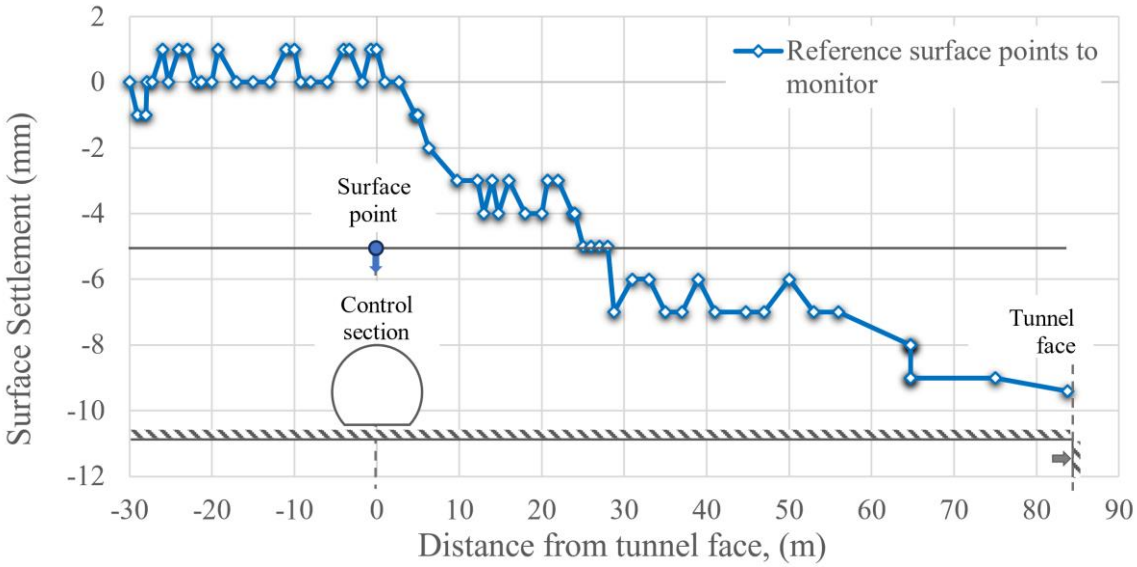

Figure 21. Surface points to monitor settlements in the control section.

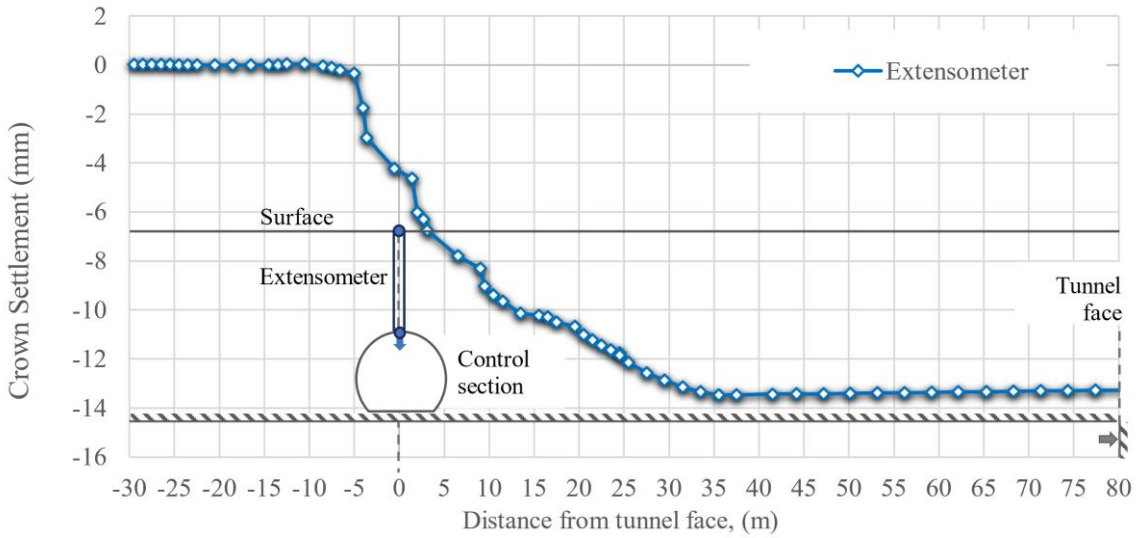

Figure 1. Extensometer measurements.

Preprints.org (www.preprints.org) | NOT PEER-REVIEWED | Posted: 16 July 2024 doi:10.20944/preprints202407.1329.v1

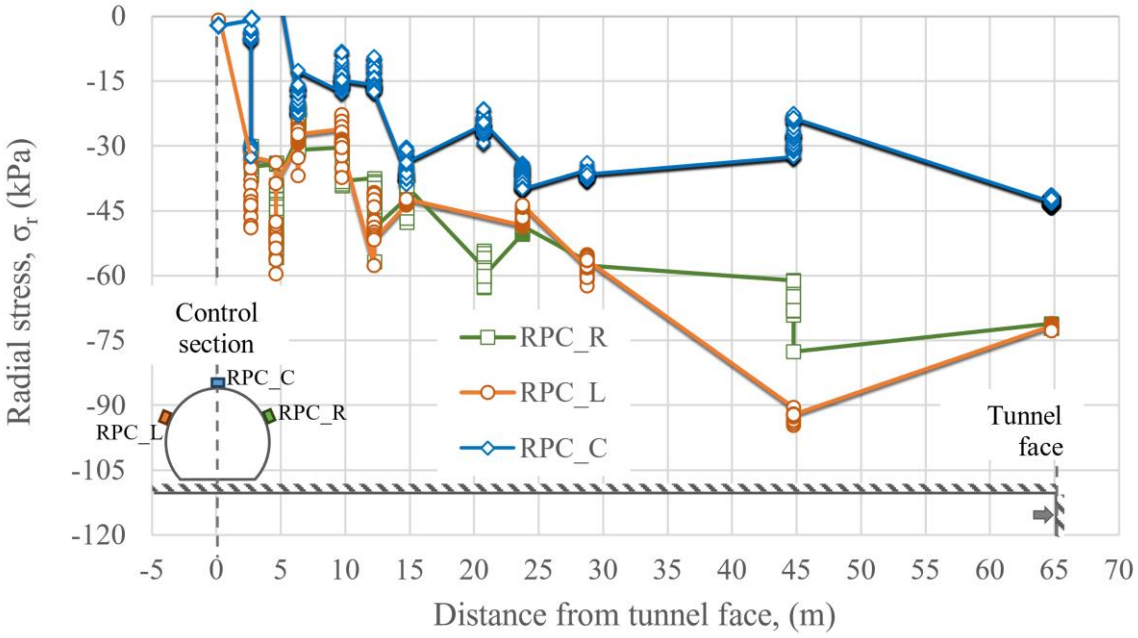

Figure 23. Recorded radial pressures.

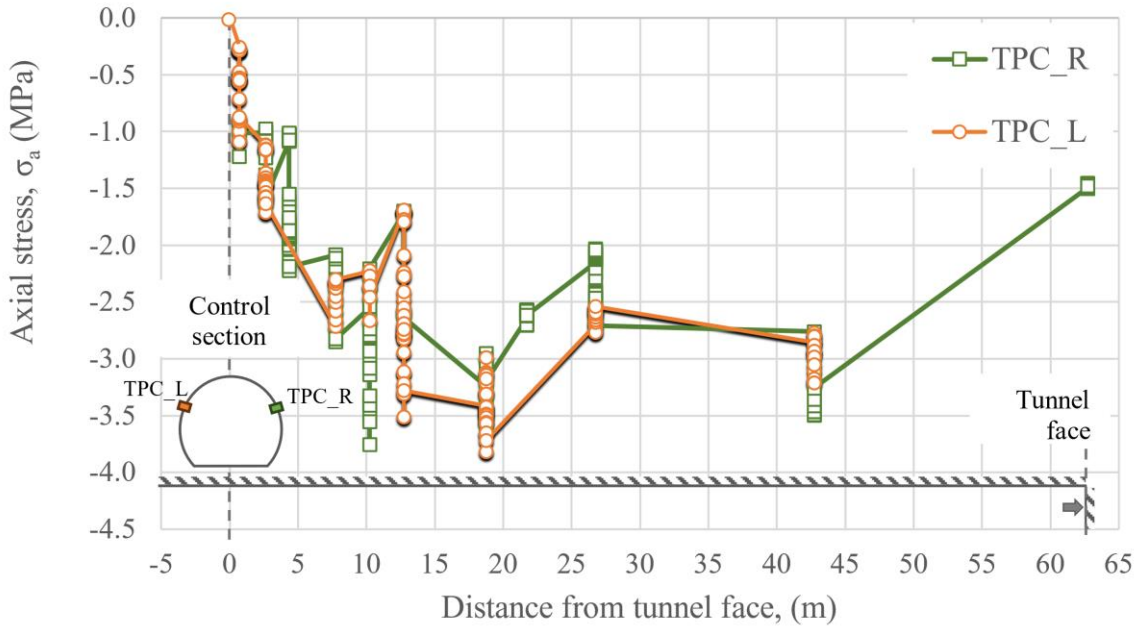

Figure 24. Recorded axial pressures.

4. Numerical Modelling

Three-dimensional finite difference numerical models were developed using the program FLAC3D (Itasca, 2009), as depicted in **Error! Reference source not found.**, to assess the load transfer mechanism in the primary and secondary lining. An elasto-plastic Mohr-Coulomb model was used to simulate the stress-strain relationship. The soil profile was idealized horizontally according to the geotechnical layering prevailing at the instrumented tunnel section (i.e., chainage 29+350 and 29+250). **Error! Reference source not found.**a shows the control points. The simulation included the construction process following the steps previously described. The primary lining, PL, was simulated using shell elements and the soil with solid elements. The model consists of 319000 three-dimensional elements representing the soil mass through which the tunnel is excavated. For the constitutive law

 doi:10.20944/preprints202407.1329.v1

of the primary lining, SRCF, a nonlinear stress-strain relationship was considered, including the evolution of the shotcrete properties with time (see **Error! Reference source not found.**), which reaches its design strength at 28 days.

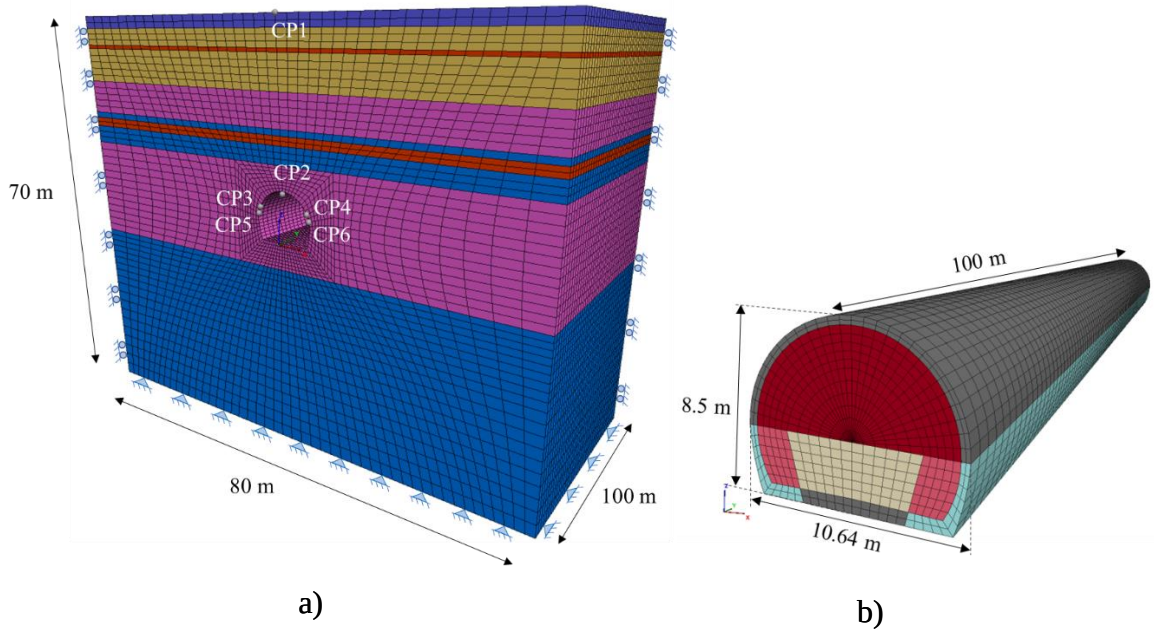

Figure 25. Three-dimensional mesh of finite differences a) global domain of the model. **b) discretization of construction stages.**

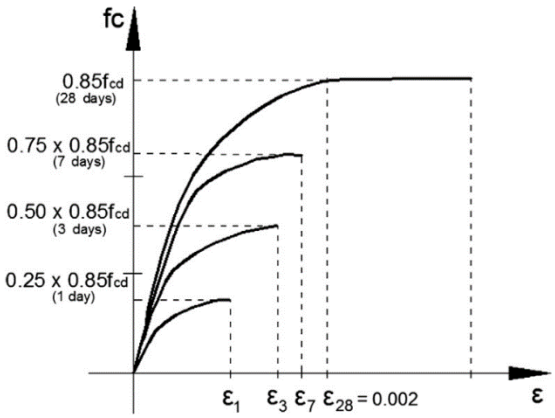

Figure 26. Evolution of SFRC stress-strength relationship over time.

4.1. Model Prediction and Back-Analyses

A blind model prediction and back-analyses were conducted to calibrate the numerical models of the analysed section. Initially, the properties shown in Table 1 were used to assess the potential foreseen capability of the model, comparing the data gathered from the instrumentation (i.e., topographic references, tunnel cross section converges and divergences, and radial and axial pressure cells), with those obtained from the numerical model. In a second step, the soil properties were adjusted slightly to better match the measured response. If there exists a discrepancy, Young's modulus, cohesion, and friction angle were adjusted accordingly to account for changes associated to the excavation process at the soil adjacent to the excavation seeking to minimize the relative error.

This step was repeated until the relative error between the computed and measured values (i.e., surface and tunnel crown settlements, radial, and axial stresses) were minimized. The final properties (i.e., obtained through the back-analysis) are also presented in **Error! Reference source not found.**.

 doi:10.20944/preprints202407.1329.v1

Table 3. Back calculated geotechnical properties at the studied site.

Layer	USCS	N_{SPT} (blows counts)	γ (kN/m³)	c (kPa)	φ (°)	E_{50} (MPa)	ν (-)
UG-1	ML	51	15.8	20.5	28	160	0.32
UG-2	SM	167	18.2	51.2	30	970	0.28
UG-3	CL-ML	40	17	15.6	27	123	0.34
UG-4	ML	126	18.2	47.5	28	590	0.28
UG-5	SC	80	19.2	36.3	32	445	0.27

Where N_{SPT}= extrapolated number of standard penetration tests blows counts; γ= unit weight; c= cohesion, φ= friction angle; E_{50}= Young's modulus at 50% strain; ν= Poisson ratio.

Error! Reference source not found. shows the displacement obtained from the numerical model and those measured at the surface with topographic survey, along with the readings from the extensometer installed from the surface to the tunnel crown. It is warranted to notice that the ground deformation at the surface is around 1 mm at the instrumented section when the excavation reaches this location, whereas at the tunnel crown it reaches 6mm. For completeness, the blind model predictions, identified as FLAC_ini, were also included in all comparisons. After the excavation front passes by the instrumented section, and abrupt deformation of both the ground surface and tunnel crown is observed. This is associated with the brittle stress-strain relationship observed in cemented silty sand and sandy silts, as depicted in **Error! Reference source not found.**, which summarizes the stress-strain curves obtained from unconfined compressions tests, UCT, of the geomaterials found in the studied site.

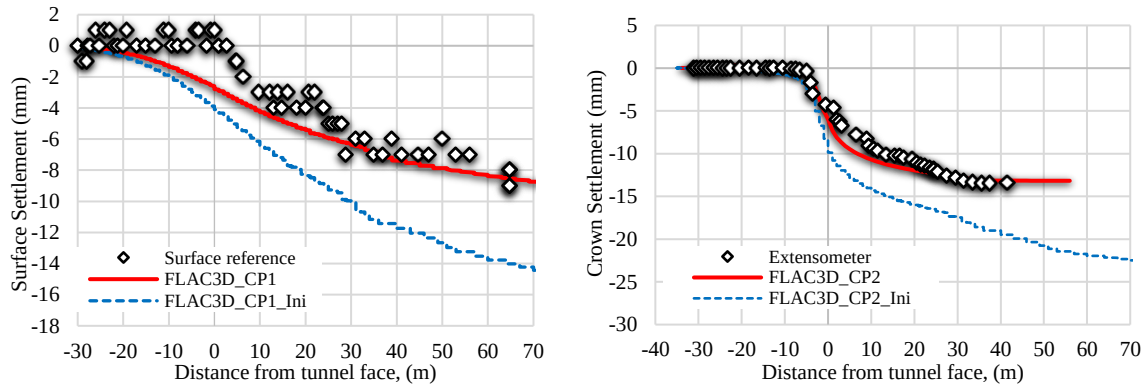

Figure 27. Settlements recorded and predicted on the surface above the tunnel axis and on the tunnel crown.

Preprints.org (www.preprints.org) | NOT PEER-REVIEWED | Posted: 16 July 2024 doi:10.20944/preprints202407.1329.v1

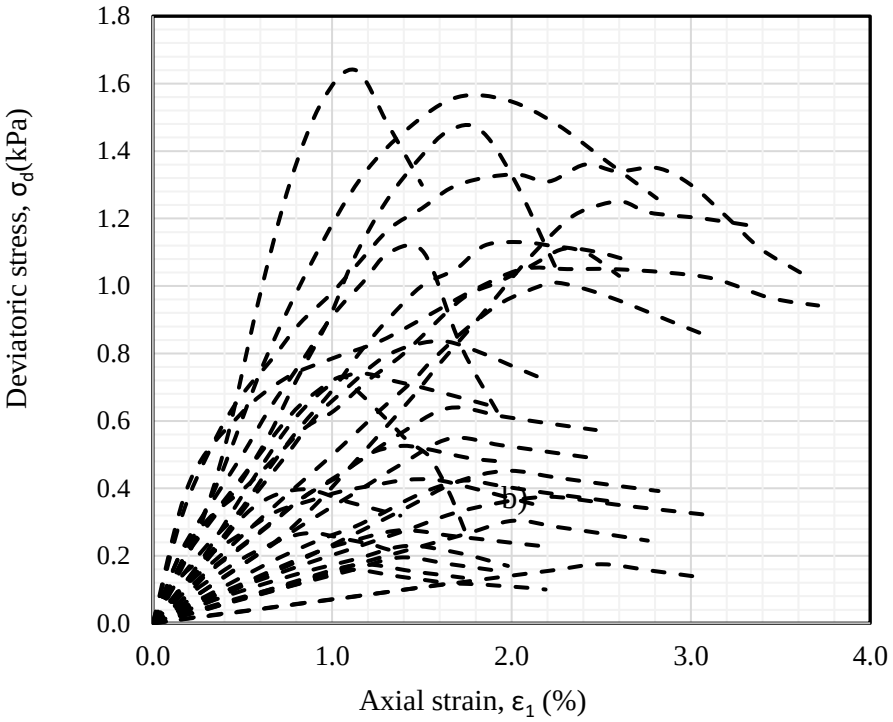

Figure 28. Unconfined compression tests stress-strain relationship of the tuff soils.

Vertical and horizontal movements at the tunnel crown and sidewalls respectively, are depicted in **Error! Reference source not found.**. As can be seen, the results obtained with the numerical model are in good agreement with those gathered from the instrumentation, where a larger displacement was obtained at the tunnel crown with respect to that horizontal displacement measured at the sidewall, as expected.

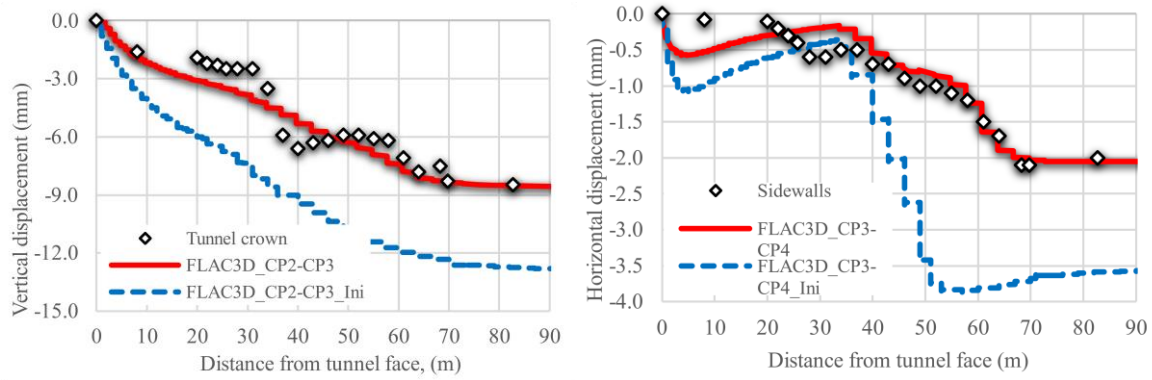

(a) (b)

Figure 29. Measured and predicted ground movements at (a) tunnel crown and (b) sidewalls respectively.

Similarly, **Error! Reference source not found.** shows the pressures measured at TPCs, and RPCs load cells located in the sidewall and the tunnel crown, and those computed with the numerical model, as can be seen the model predictions are in good agreement with the measured response.

Preprints.org (www.preprints.org) | NOT PEER-REVIEWED | Posted: 16 July 2024 doi:10.20944/preprints202407.1329.v1

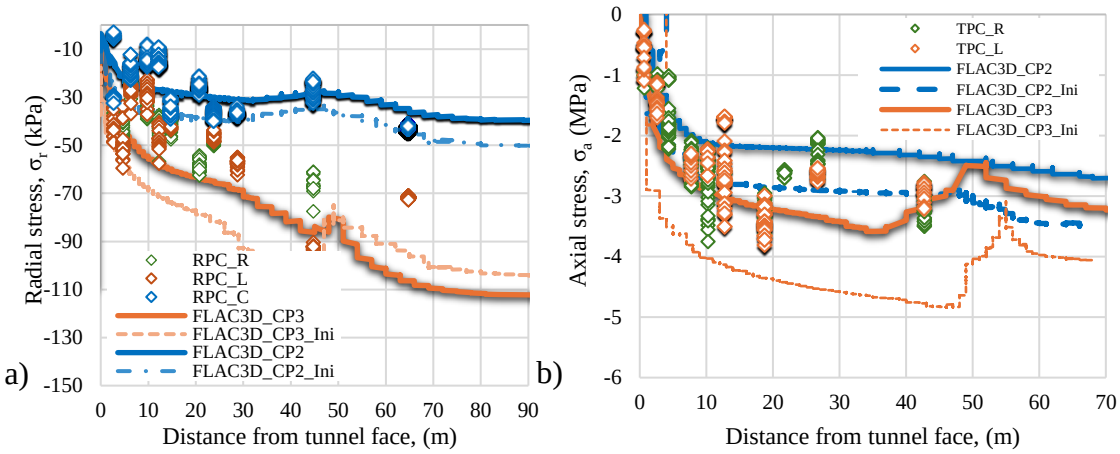

Figure 30. Pressures measured and predicted on the primary lining a) radial b) axial.

The measured and computed convergences at the secondary lining after its construction are shown in **Error! Reference source not found.**. As can be noticed, there is a good agreement between computed and measured response. Thus, the numerical model is able to foresee the measured secondary lining performance very closely for all cases.

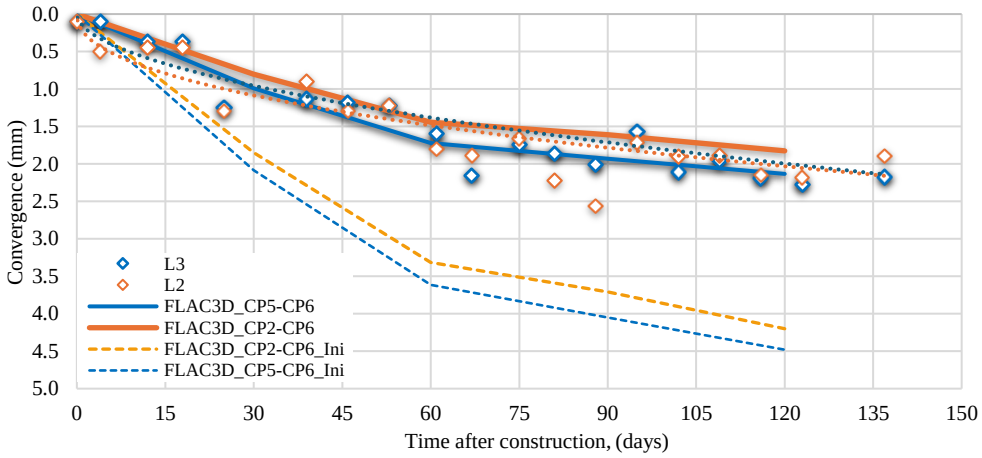

Figure 31. Measured and predicted convergences at the monitoring section in the secondary lining.

5. Comparison with Analytical Methods

Very often, simplified methods such as those based on the development of ground softening pressure on the tunnel vault (Bierbaumer, 1913; Terzaghi, 1946) may lead to costly designs and unsafe scenarios during tunneling execution. Those design approaches ignore the actual soil-tunnel lining interaction mechanism, and therefore they should be only used in preliminary tunnel design. Other design approach often used to estimate lining pressures approximately, which attempt to account for soil-tunnel lining interaction and deformations are the so-called Convergence-Confinement method, CCM (Panet and Guenot, 1983). This methodology is based on the development of the ground reaction curve, GRC, and the support reaction curve, SRC, which allows the calculation of the stress relief due to soil unconfinement during excavation, and the estimation of deformations around the tunnel in the sequence of lining installation, as the excavation continues gradually (Alonso, 2003; Oreste, 2009). CCM allows to compute the radial pressure acting on the primary lining, which is defined as the intersection between the GRC and the SRC curves. In this way, only the pressure that has not yet been redistributed in the ground is considered as active pressure on the lining. To obtain the corresponding displacement to that stress redistribution, it is necessary to calculate another curve, called conventionally Longitudinal Displacement Profile, LDP, which provides the displacement expected around the tunnel as the excavation face is approaching to the control section and the

 doi:10.20944/preprints202407.1329.v1

displacement as the excavation face moves away from the control section. Although this is a more reasonable way to obtain the lining pressures, most of the existing equations has been derived to very idealized conditions, (e.g., isotropic stress field K_0=1, circular tunnel cross sections, one excavation stage, plane-strain conditions). **Error! Reference source not found.**b shows the GRC and the SRC curves, calculated with the equations proposed by several authors, as well as the calculated with the calibrated model in FLAC^{3D} accounting for the support installation, on the crown and on the sidewalls. The average GRC curve includes the computed curves from Stille et.al, (1989); Tamez, (1997); Alonso, (2003); and Oreste, (2009) which led to similar results, because they consider initial properties, on the other hand the curve from Fairhust (1991) predicted larger displacement values because it accounts for residual strength parameters in the plastic region around the tunnel. **Error! Reference source not found.**a shows the LDP curve, as well as the pre-convergence displacement, u_0/u_{max}.

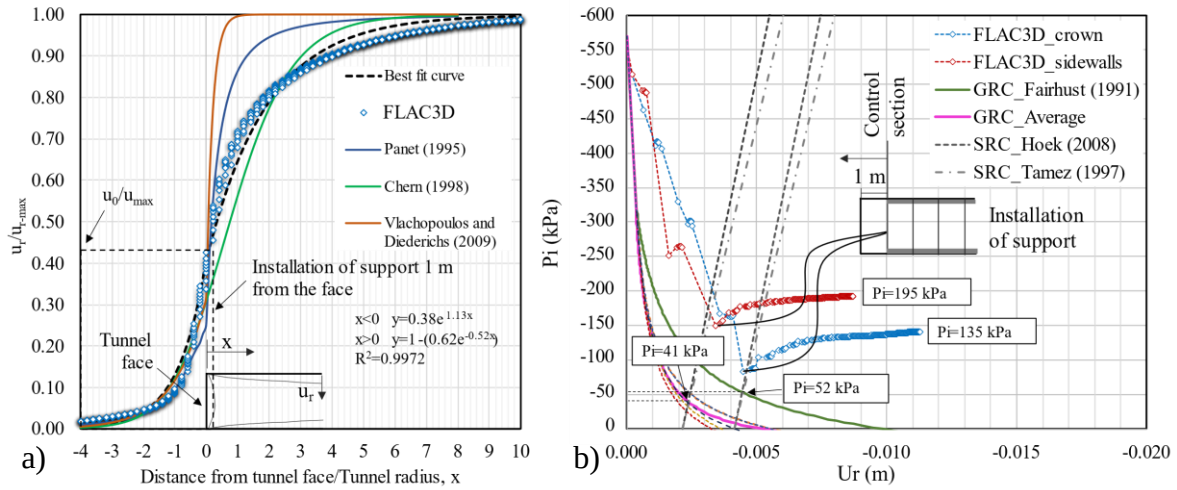

Figure 32. a) Ground reaction and support reaction curves, calculated with analytical methods and with the calibrated numerical model, and b) longitudinal displacement profiles, LDP, calculated with analytical methods and with the calibrated numerical model.

As can be seen, all the analytical models considered underestimate both ground displacement and pression distribution acting on the primary lining. This is a major source of ground settlement during tunnel construction that can easily exceed the state limits of service of nearby structures in urban areas. Furthermore, differential settlements associated with this fact can potentially lead to structural damage of adjacent structures. In addition, in **Error! Reference source not found.**a, the fitted curve from the calibrated numerical model exhibits a different behavior than the other proposed equations derived from several measured data (Chern, 1998), elastic analysis (Panet, 1995), and numerical models (Vlachopoulos and Diederichs, 2009). This behavior can be attributed to the idealized conditions considered to derive the equations to computed GRC and LDP, (i.e., circular tunnel cross section, and the assumption of K_o=1). **Error! Reference source not found.** shows the displacement contours around the tunnel, considering the idealized conditions of the CCM (**Error! Reference source not found.**a), and the real conditions from the calibrated numerical model (**Error! Reference source not found.**b). The main difference is that the displacement distribution is strongly affected by the vertical component, and not the radial deformations as assumed in the CCM curves.

 doi:10.20944/preprints202407.1329.v1

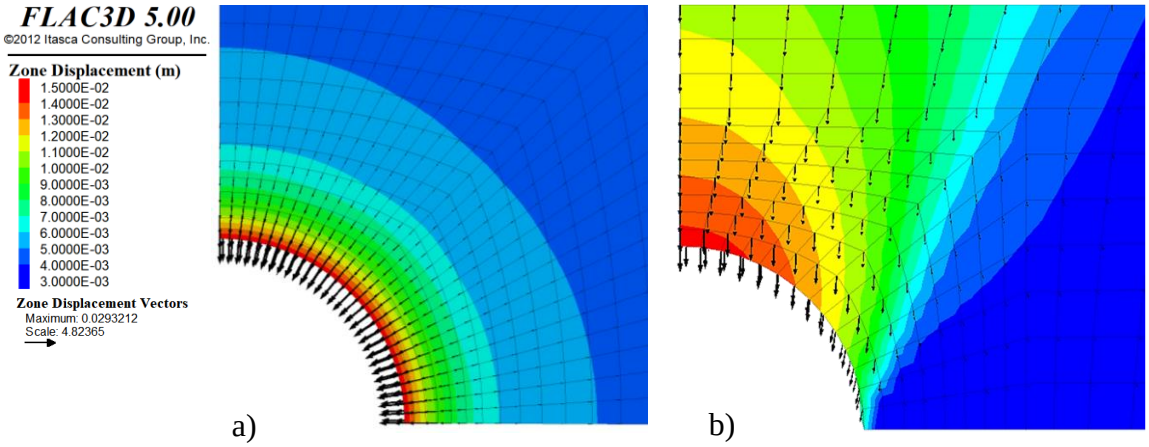

Figure 33. Displacements contours around the tunnel calculated with a) the idealized conditions of the analytical methods, and b) real conditions of the calibrated numerical model.

6. Optimization of Tunnel Lining Performance

In order to study the sensitivity of the primary and secondary lining thickness on the tunnel performance, a parametric analysis was conducted. Four different cases were considered, as summarized in **Error! Reference source not found.**. The lining performance was established based on interaction diagrams (Kaiser, 1985; Sauer, et al., 1994; Mayoral et al., 2020), comparing the computed bending moment and the normal force (M-N) combination with the limit defined by the boundary in the interaction diagram. These diagrams are a simplified graphical representation of the critical fault surface, separating acceptable load combinations and those that exceed the allowed limits. The σ-ε method was used to derive the interaction M-N diagrams (i.e., bending moment-normal force) (Sauer, et al. 1994; Vandewalle, 2000). **Error! Reference source not found.**a and **Error! Reference source not found.**b, shows the constitutive model considered for the secondary lining, (i.e., concrete and steel bars, respectively), and **Error! Reference source not found.**c, the constitutive model for the primary lining (i.e., shotcrete reinforced with steel fibers) where it can be seen the contribution of the steel fibers in the tension portion of the curve.

Table 4. Cases of primary lining thickness analyzed.

Case	Primary lining thickness (m)	Secondary lining thickness (m)
1	0.2	0.4
2	0.3	0.3
3	0.4	0.2
4	0.6	---

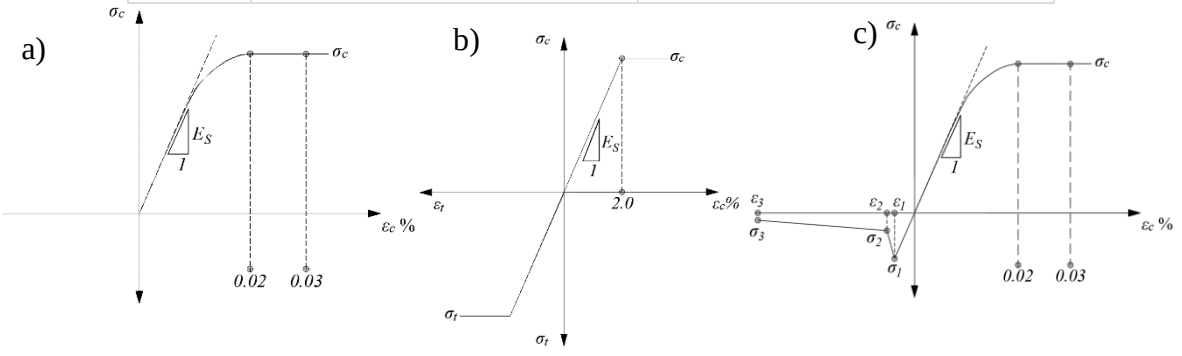

Figure 34. Constitutive laws used in the definition of interaction diagrams a) concrete b) steel bars, and c) steel fiber reinforced shotcrete (SFRS).

 doi:10.20944/preprints202407.1329.v1

Error! Reference source not found.a and **Error! Reference source not found.**b shows the interaction diagrams and acting forces on the first three cases, on the primary and secondary linings, respectively. In all cases, the acting forces on the secondary lining are minimal and are concentrated in the center of the diagram. On the other hand, the acting forces on the primary lining are more important, nevertheless they still have a good safety factor gap, which is more evident in the case with the primary lining thickness of 60 cm (**Error! Reference source not found.**). In addition, **Error! Reference source not found.** shows the surface vertical displacement profiles in a cross-section perpendicular to the tunnel axis, from all the studied cases. As expected, with the primary lining thickness of 60 cm the magnitude of settlements is minor even without the secondary lining, which in this case has a negligible contribution. These results suggest that the best alternative for tunneling in these types of materials is the use of only one robust lining, because it can support the forces from the ground stress redistribution during tunneling while decreasing the impact of the excavation on the surface. Such as alternative has been used in past tunnel projects in nearby zones with similar geotechnical conditions (Tamez, et al., 1997), and around the world (Barton, 2017; Li et al., 2023), highlighting its rapid construction as well as its practical installation compared to a composite lining. Although several problems have been identified in the usage of single linings, like high temperatures during strength gaining, high deformation, and shrinkage (Haack, 1988), it has been observed that these limitations can be overcome if the lining is sprayed in two to three layers (Pickett & Thomas, 2013).

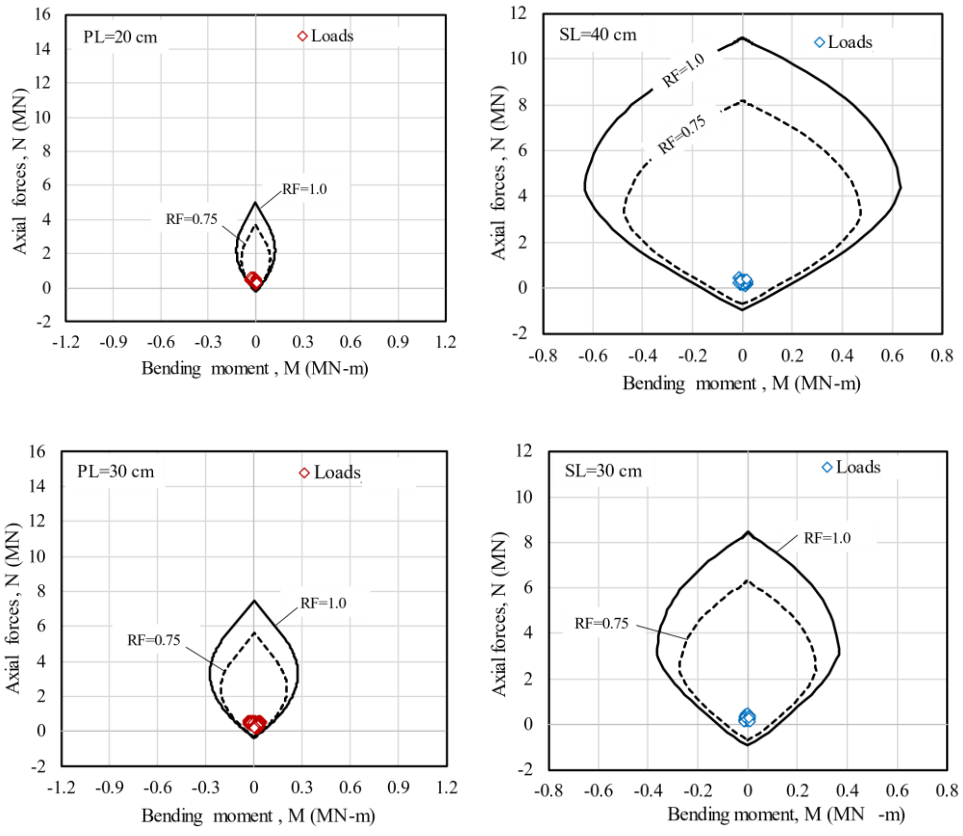

Preprints.org (www.preprints.org) | NOT PEER-REVIEWED | Posted: 16 July 2024 doi:10.20944/preprints202407.1329.v1

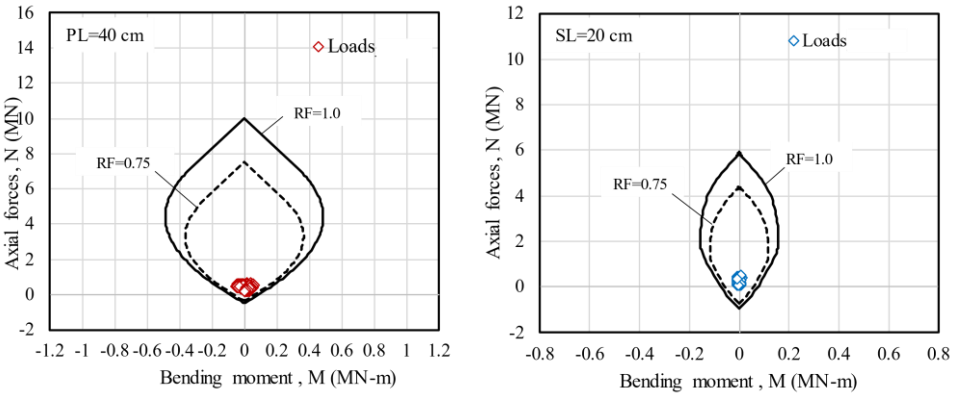

(a) (b)

Figure 35. Interaction diagrams and acting loads at (a) the primary lining and (b) secondary lining.

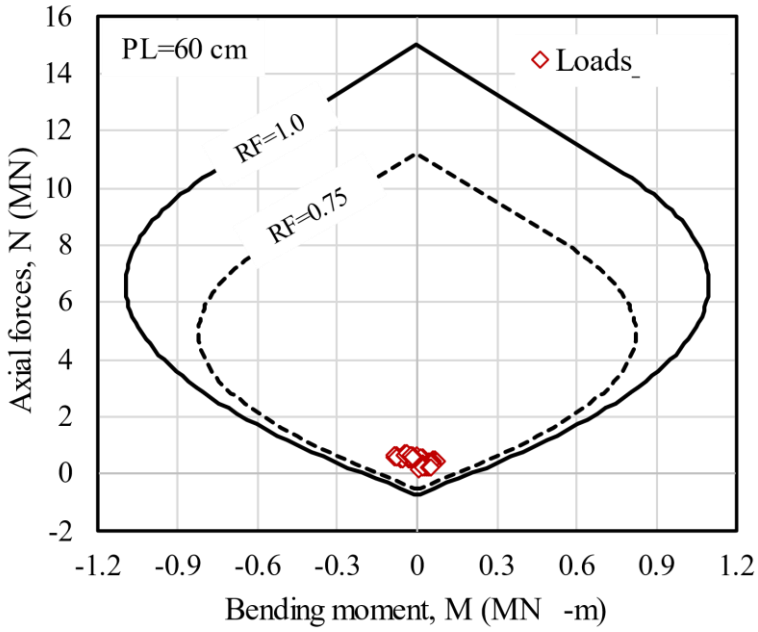

Figure 36. Interaction diagram and acting loads at primary lining.

 doi:10.20944/preprints202407.1329.v1

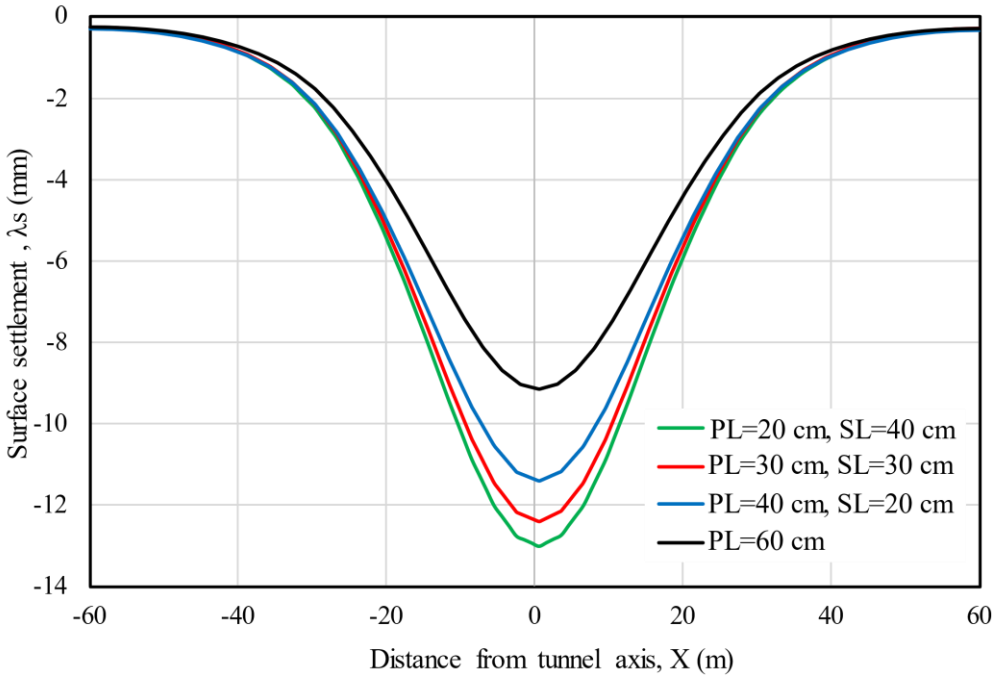

Figure 37. Surface vertical displacements perpendicular to the tunnel axis for each case analyzed.

7. Conclusions

Modern tunnel lining design must include the revision of state limits of failure and service simultaneously using a performance base design approach. In urban areas this is a key step to effectively reduce ground movement of the tunnel surrounding soil, which in turn, can led to differential settlements on adjacent structures, and potential structural damage. This paper is aimed at partially filling the gap of field data regarding the load distribution acting on primary linings during conventional tunnelling. An extensive instrumentation of a section of a tunnel of a 4.5km long metro currently under construction on the north-western area of Mexico City was carried out. The instrumentation was comprised of load cells to measured radial and axial pressures in the primary lining, an extensometer, topographical survey points at the ground surface, and convergence and divergences readings of the tunnel cross section. The presented results are further analysed with three-dimensional finite difference numerical models. From both experimental and numerical data gathered it can be clearly seen that the traditional analytical models under predict substantially both ground deformations as well as design loads in the primary lining. This is most likely due to the hypothesis employed to derive these analytical solutions, such as circular tunnel cross section, uniform isotropic stress field, among others. It is important to highlight that in the horseshoe tunnel geometry studied in here, the displacement distribution is strongly affected by the vertical component, and not by radial deformations as assumed in the CCM approaches revised. Therefore, the lining performance design following these procedures is not optimal, and can potentially lead to unsafe and costly designs, and in extreme cases, damage to surrounding structures. Special care should be exercise in brittle soils, such as cemented sandy silts and silty sands, which exhibits a strain softening behaviour, and in which the failure surface is reached at relatively small ground deformations, precluding catastrophic collapses. Underprediction of the equilibrium tunnel crown vertical deformation on the order of one third of the measured deformation was observed. Loads inferred in the secondary lining based on the back calibrated numerical model are almost one tenth of those taken by the primary lining. This fact can be attributed to the brittleness of the cemented silty sands, which lead to the fact that approximately 70 to 90% of the soil load is taken by the primary lining during the initial excavation advance, prior to the construction of the secondary lining. Thus, from the numerical study presented in here, it can be concluded that it is more efficient in urban populated areas, when using the conventional tunnelling method in stiff cemented soils, to have a

 doi:10.20944/preprints202407.1329.v1

robust lining that allows a better control of the ground deformation, less detrimental impact in adjacent structures, and a faster construction, than a support comprised of primary and secondary lining. Therefore, one robust lining can support the surrounding soil loads, redistribute the soil stresses around the tunnel during excavation, and decreasing the impact on the surface. Both state limits of failure and service are to be revised during the design phase. Using empirical and analytical approaches should be restricted to preliminary estimations.

Author Contributions: Conceptualization, Juan-Manuel Mayoral Villa and José-Francisco Suarez-Fino; Methodology, Juan-Manuel Mayoral Villa and José-Francisco Suarez-Fino; Writing – original draft, Juan-Manuel Mayoral Villa and José-Francisco Suarez-Fino.

Funding: This research has been funded by the Engineering Institute of the National Autonomous University of Mexico.

Conflicts of Interest: The authors declare no conflict of interest.

References

1. Alonso, E., 2003. Ground response curves for rock masses exhibiting strain-softening behavior. International Numerical Analyses Meth. Geomech, Volumen 27, pp. 1153-1185.
2. de Ágreda, E. A. P. (2019). Failures Inspire Progress: Protecting Sensitive Buildings from Tunnelling. GeoStrata Magazine Archive, 23(5), 34–39.
3. Argyroudis, S., Tsinidis, G., Gatti, F., Pitilakis, K., 2017. Effects of SSI and lining corrosion on the seismic vulnerability of shallow circular tunnels. Soil Dynamics and Earthquake Engineering 98 (2017) 244–256
4. Behnen, G., Nevrly, T., Fischer, O., 2015. Soil-structure interaction in tunnel lining analyses. geotechnik 38, 96–106. https://doi.org/10.1002/gete.201400010
5. Bierbaumer AH (1913) Die dimensionierung des tunnel manerwerks.Liepzig, Germany
6. Bin, L., 2016. Reliability Analysis of Primary Supports in Deep and Soft-rock Tunnel Based on Probabilistic Design Numerical Method. Electron. J. Geotech. Eng. 5013–5028.
7. Chern, J.C., Shiao, F.Y., Yu, C.W., (1998) An empirical safety criterion for tunnel construction. Proceedings of the Regional Symposium on Sedimentary Rock Engineering, Taipei, Taiwan,pp 222–227
8. Dong, Z., Zhang, X., Tong, C., Chen, X., Feng, H., Zhang, S., 2022. Grouting-induced ground heave and building damage in tunnel construction: A case study of Shenzhen metro. Underground Space 7 (2022) 1175–1191.
9. Einstein, H. H., & Schwartz, C. W. (1979). Simplified Analysis for Tunnel Support. Journal of the Geotechnical Engineering Divison, 105, 499–518.
10. Fairhurst, C., 1991. General philosophy of support design for underground structures in hard rock. Underground Structures. Design and Construction, pp. 1-55.
11. Ghorbani, A., & Hasanzadehshooiili, H. (2019). A comprehensive solution for the calculation of ground reaction curve in the crown and sidewalls of circular tunnels in the elastic-plastic-EDZ rock mass considering strain softening. Tunnelling and Underground Space Technology, 84(November 2018), 413–431. https://doi.org/10.1016/j.tust.2018.11.045
12. Guo, X., Du, D., Dias, D., 2019. Reliability analysis of tunnel lining considering soil spatial variability. Eng. Struct. 196, 11. https://doi.org/10.1016/j.engstruct.2019.109332
13. Hamrouni, A., Dias, D., Sbartai, B., 2017. Reliability analysis of shallow tunnels using the response surface methodology. Undergr. Sp. 2, 246–258. https://doi.org/10.1016/j.undsp.2017.11.003
14. He, B.M., Zhang, X.W., Li H.P., 2019. Ground load on tunnels built using new Austrian tunneling method: study of a tunnel passing through highly weathered sandstone. Bulletin of Engineering Geology and the Environment volume 78, pages6221–6234 (2019)
15. Hettiarachchi, H. & Brown, T., 2009. Use of SPT Blow Counts to Estimate Shear Strength Properties of Soils: Energy Balance Approach. Journal of Goetechnical and Geoenviromental Engineering ©ASCE, pp. 830-834
16. ITA, 2009. General Report on Conventional Tunnelling Method 27.
17. Itasca Consulting Group. FLAC, Fast Lagragian Analysis of Continua. User's guide. Menneapolis, Minnesota, USA; 2009.
18. Kaiser, P., 1985. Rational assessment of tunnel liner capacity. Montreal, Proceedings of the 5th Canadian Tunneling Conference.
19. Karakus, M., Fowell, R.J., 2005. Back analysis for tunnelling induced ground movements and stress redistribution, Tunnelling and Underground Space Technology 20 (2005) 514–524.
20. Lim, C.X., Jusoh, S.N., Lim, C.B., Abdullah, R.A., Yunus, N.Z.M., 2023. Tunnel depth effect to pile in Tunnel's influence zone. Physics and Chemistry of the Earth 129 (2023) 103298.

21. LRFD Bridge Design Specifications (2012) American Association of State Highway and Transportation Officials (AASHTO).
22. Mayoral, J. M. (2014). Performance evaluation of tunnels built in rigid soils. Tunnelling and Underground Space Technology, 43, 1–10. https://doi.org/10.1016/j.tust.2014.03.013
23. Mayoral, J. M., Melis-Maynar, M. J. I., & de la Sancha, A. R. (2015). Integral Approach of Performance-Based Design for Tunnels. Transportation Research Record: Journal of the Transportation Research Board, 2522, 121–130. https://doi.org/10.3141/2522-12
24. Mayoral, J.M., Mosqueda, G., De La Rosa, D., Alcaraz, M., 2020. Tunnel performance during the Puebla-Mexico 19 September 2017 earthquake. Earthq. Spectra 36, 288–313. https://doi.org/10.1177/8755293020976140
25. Mayoral, J. M., & Mosqueda, G. (2021). Foundation enhancement for reducing tunnel-building seismic interaction on soft clay. Tunnelling and Underground Space Technology, 115(August 2020), 104016. https://doi.org/10.1016/j.tust.2021.104016
26. Mayoral, J. M., Alcaraz, M., & Tepalcapa, S. (2023). Seismic performance of soil–tunnel–building systems in stiff soils. Earthquake Spectra, 39(2), 1214–1239. https://doi.org/10.1177/87552930231168165
27. Ng, C.W.W., Lu, H., Peng S.Y. Three-dimensional centrifuge modelling of the effects of twin tunnelling on an existing pile. Tunnelling and Underground Space Technology 35 (2013) 189–199.
28. Nomoto, T., Imamur, S., Hagiwara, T., Kusakabe, O., Fujii, N., 1999. Shield Tunnel Construction in Centrifuge. Journal of Geotechnical and Geoenvironmental EngineeringVolume 125, Issue 4Apr 1999Pages237-345.
29. Oliver, A. (1994). Heathrow trial runs under question. New Civil Engineer, 4–5.
30. Oliver, A. (1995). Rush to stabilise Heathrow chasm. International Journal of Rock Mechanics and Mining Sciences and Geomechanics Abstracts, 4(32), 189A.
31. Oreste, P. P. (2003). A Procedure for Determining the Reaction Curve of Shotcrete Lining Considering Transient Conditions. Rock Mechanics and Rock Engineering, 36(3), 209–236. https://doi.org/10.1007/s00603-002-0043-z
32. Oreste, P. (2009). The convergence-confinement method: Roles and limits in modern geomechanical tunnel design. American Journal of Applied Sciences, 6(4), 757–771. https://doi.org/10.3844/ajas.2009.757.771
33. Panet M (1995) Calcul des Tunnels par la Me'thode de Convergence–Confinement. Presses del'Ecole Nationale des Ponts et Chausse'es, Paris, 178 p
34. Panet, M., Bouvard, A., Dardard, B., Dubois, P., Givet, O., Guilloux, A., Launay, J., Duc, N.M., Piraud, J., Tournery, H., Wong, H., (2001). The Convergence-Confinement Method. AFTES–recommendations des Groupes Travait.
35. Panet, M., & Guenot, A. (1983). Analysis of convergence behind the face of a tunnel : Tunnelling 82, proceedings of the 3rd international symposium, Brighton, 7–11 June 1982, P197–204. Publ London: IMM, 1982. International Journal of Rock Mechanics and Mining Sciences & Geomechanics Abstracts, 20.
36. Pitilakis, K., Tsinidis, G., Leanza, A., & Maugeri. M., (2014). Seismic behaviour of circular tunnels accounting for above ground structures interaction effects. Soil Dynamics and Earthquake Engineering 67 (2014) 1–15
37. Sadeghiyan, R., Hashemi, M., & Moloudi, E. (2016). Determination of longitudinal convergence profile considering effect of soil strength parameters. International Journal of Rock Mechanics and Mining Sciences, 82, 10–21. https://doi.org/10.1016/j.ijrmms.2015.10.011
38. Sauer, G., Gall, V., Bauer, E. & Dietmaier, P., (1994). Design of tunnel concrete linings using limit capacity curves. Computers Methods and Advances in Geomechanics, pp. 2621-2626.
39. Son, M., (2015). Response analysis of nearby structures to tunneling-induced ground movements in sandy soils. Tunnelling and Underground Space Technology 48 (2015) 156–169.
40. Son, M., (2016). Response analysis of nearby structures to tunneling-induced ground movements in clay soils. Tunnelling and Underground Space Technology 56 (2016) 90–104.
41. Song, G., ;arshall A.M., (2020). Centrifuge modelling of tunnelling induced ground displacements: pressure and displacement control tunnels. Tunnelling and Underground Space Technology Volume 103, September 2020, 103461
42. Sousa, R. L., & Einstein, H. H. (2021). Lessons from accidents during tunnel construction. Tunnelling and Underground Space Technology, 113. https://doi.org/10.1016/j.tust.2021.103916
43. Stille, H., Holmberg, M. & Nord, G., (1989). Support of weak rock with grouted bolts and shtocrete. Internatinal Journal on Rock Mechanics, Min. Sci., 26(1).
44. Szechy K (1970) The art of tunnelling. Akademiai Kaido, Budapest.
45. Tamez, E., Rangel, J. L. y Holguin, E., 1997. Diseño geotécnico de túneles. Diseño geotécnico de túneles: TGC Geotecnia. In Spanish.
46. Terzaghi K (1946) Introduction to tunnel geology in rock tunneling withsteel supports. Youngstown, Ohio, USA

 doi:10.20944/preprints202407.1329.v1

47. Vandewalle, L. (2000). Recommendations of RILEM TC 162-TDF: Test and design methods for steel fibre reinforced concrete. Materials and Structures/Materiaux et Constructions, 33(225), 3–5.
48. Verman, M., Singh, B., Jethwa, J. L., & Viladkar, M. N. (1995). Determination of Support Reaction Curve for Steel-Supported Tunnels.
49. Vlachopoulos, N., Diederichs, M. S. (2009). Improved Longitudinal Displacement Profiles for Convergence Confinement Analysis of Deep Tunnels. Rock Mechanics and Rock Engineering, 42(2), 131–146. https://doi.org/10.1007/s00603-009-0176-4
50. Wang, Y. Q., Luo, M. R. (2020). Analysis of Support Reaction Curves considering Time-Varying Effect of Shotcrete. Advances in Civil Engineering, 2020. https://doi.org/10.1155/2020/6069432
51. Wood, D., 2004. Geotechnical Modelling. s.l.:Taylor y Francis.
52. Zhang, D., Fang, Q., Li, P., Wong L.N.Y., 2013. Structural Responses of Secondary Lining of High-Speed Railway Tunnel Excavated in Loess Ground Adv Struct Eng 16:1371–1379. https://doi.org/10.1260/1369-4332.16.8.1371.